Supplementary Information

A Single AT-GC Exchange Can Modulate Charge Transfer-Induced p53-DNA Dissociation

Ruijie D. Teo,[†] Elizabeth R. Smithwick,[†] Agostino Migliore,[†,*] David N. Beratan[†,‡,§,*]

[†] Department of Chemistry, Duke University, Durham, North Carolina 27708, United States

[‡] Department of Biochemistry, Duke University, Durham, North Carolina 27710, United States

[§] Department of Physics, Duke University, Durham, North Carolina 27708, United States

Contents

Section S1 details the molecular dynamics (MD) simulations of the p53-DNA complexes. Sections S2-S3 describe the calculations of the electronic couplings, reorganization energies and associated parameters, such as the center-to-center distance R_{DA} between the hole donor (*D*) and acceptor (*A*), and the effective radii of purine nucleobases. These parameters were inserted into eqn (1) to obtain the CT rate constant for each charge transfer (CT) step in Fig. 2. The resulting parameters and rate constants are reported in Section S4.

S1. MD simulations

The MD simulations of the protein-DNA systems described in Fig. 1 were carried out using the NAMD 2.11 software.[1] We used the Zinc AMBER force field (ZAFF)[2] to parameterize the four-coordinated zinc center in p53, the ff14SB[3] and ff99-bsc0[4, 5] AMBER force fields for the protein

and DNA, respectively. Both p53-Gadd45 DNA and p53-p21 DNA systems were neutralized using K^+ ions and solvated with a box of TIP3P water[6] extending 10 Å on each side of the protein-DNA complex. The resulting unit cell vectors were (in Å): (**100.334**, **90.16**, **100.36**).

The SHAKE algorithm[7] was used to constrain H-O and H-H distances in the water molecules. Full electrostatics evaluation was carried out every two time steps. The effective electrostatic potentials were calculated using the particle mesh Ewald summation method,[8] with grid spacing of 1 Å. The scaling factor for 1-4 electrostatic interactions was set to 0.833333. The van der Waals interactions were truncated at a cutoff distance of 12 Å. The list of non-bonded atoms to be considered for the periodic interaction energy calculation included atomic pairs within 14 Å.

Both solvated protein-DNA complexes were subject to 80000 energy minimization steps, followed by solvent equilibration (using Langevin Dynamics with a damping coefficient 1.0 ps^{-1}) with fixed protein-DNA atoms at temperatures of 293 K (which is the original crystallization temperature of the p53-DNA complex in the PDB with code 2ADY[9]) for 225 ps, 295 K for 50 ps, 297 K and 298 K for 50 ps each. Then, the atoms of the p53-DNA complex were gradually released through 2.5 ns of NPT dynamics with Nosé-Hoover Langevin piston pressure control (pressure = 1 atm, 298 K, barostat oscillation period = 100 fs, damping time scale = 50 fs, damping coefficient = 2.0 ps^{-1}). The DNA backbone, the S atoms of the C277 residues linking to DNA, Zn, and the atoms coordinated to Zn were fixed during the first ns (time step = 1.0 fs); the C1' atoms of the bp triplets at the Cys-DNA contacts (Fig. 2), the C_β atoms of the C277 residues linking to DNA, Zn, and the atoms coordinated to Zn remained fixed in the next ns (time step = 1.0 fs); and all atoms were finally released during the remaining 0.5 ns (time step = 0.5 fs).

The unconstrained MD production run lasted 40 ns, with a time step of 0.5 fs. The fluctuations of the RMSD for both Gadd45 and p21 systems spanned a range of about 1.06 Å (Fig. S1). For each

protein-DNA system, we disregarded the first 10 ns of MD, and extracted a snapshot every 2.5 ns in the time window 10-40 ns. The 13 snapshots selected were pruned around the two C277 residues (maintaining a methanethiol model of Cys and the triplet of nearby base pairs without the backbone) for the density functional theory (DFT) calculation of the parameters in eqn (2) and the net charge distribution on the different molecular moieties (see Sections S2 and S3).

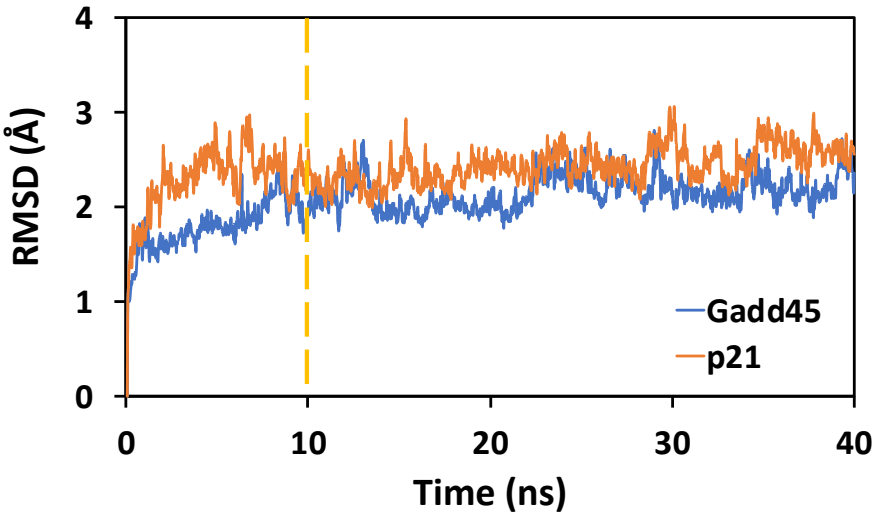

Fig. S1 RMSD (without hydrogens) along the MD production run for the protein-DNA complexes containing the Gadd45 (blue) and p21 (orange) DNA models. The MD snapshots for DFT analysis were selected starting from 10 ns (yellow dashed line).

S2. Electronic couplings

In each MD snapshot, the dangling bonds of the pruned portion were saturated by H atoms, whose positions were then relaxed by DFT geometry optimization with the B3LYP[10] density functional and the 6-31g* basis set. The electronic couplings (V_{IF}) between the Cys moiety and each DNA nucleobase pair (bp) in the contact bp triplet, as well as the couplings between adjacent bps, were calculated using eqn (2).[11, 12] For each electron-hole donor (*D*)-acceptor (*A*) pair, the initial (*I*) and

final (*F*) diabatic electronic states were obtained from calculations on the entire *D-A* system with constrained Density Functional Theory (CDFT),[13, 14] as formulated in refs. 15, 16 and implemented in the NWChem code.[17] We never needed to use the second expression in eqn (2). This expression is valid exactly at the transition state coordinates, which always represent a zero-measure subspace of the conformational space and which never accidentally occurred in any of the selected MD snapshots. Moreover, the first expression in eqn (2) can also be used, with high accuracy,[12] near the transition state coordinates (namely, where $\Delta E_{IF} \ll 2V_{IF}$,) and has a removable discontinuity exactly at such coordinates. As is shown in ref. 12, eqn (2) enables use of CDFT states to describe CT systems also when such electronic states have a partial CT character[18] that is reflected in a large diabatic state overlap, as long as the two-state approximation is satisfied.[11, 12] In addition, since only the diabatic energy difference appears in eqn (2), the DFT implementation of this formula is robust with respect to basis set superposition errors.[19]

The electronic coupling values obtained using the M11 exchange-correlation functional[20] and the 6-311g** basis set are reported in Tables S1 (for the complex between the top p53 protein and the Gadd45 model sequence), S3 (bottom p53, Gadd45), S5 (top p53, p21), and S7 (bottom p53, p21). The electronic coupling values versus the MD snapshot times are also diagrammed in Fig. S2-S5. Table S2, S4, S6, and S8 list the corresponding norms of the ground state as expanded in the CDFT diabatic set ($N = \sqrt{a^2 + b^2 + 2abS_{IF}}$), which measure the quality of the two-state approximation. The values of $\langle V_{IF} \rangle$ and $\langle {V_{IF}}^2 \rangle$ over the MD snapshots for each system are summarized in Table S9. The full Hartree-Fock-type exchange in the long-range component of the M11 functional plays a key role (especially for the farther C277 and bp redox partners, compared to the bp dimers) in avoiding electron self-interaction issues[21] that would otherwise cause a significant overestimation of the electronic couplings,[22] as it is also shown in a recent study.[23]

Table S1 Electronic coupling (V_{IF}) values (in meV) for hole transfer in the AT-Cys, GC-Cys, CG-Cys, AT-GC and GC-CG dimers, in the selected MD snapshots of the top p53-Gadd45 DNA model.

Time (ns)	AT-Cys	GC-Cys	CG-Cys	AT-GC	GC-CG
10.0	1.33×10^{1}	1.64×10^{2}	1.91×10^{1}	7.22×10^{1}	1.89
12.5	2.40	7.76×10^{-1}	1.31×10^{1}	7.94×10^{1}	3.71
15.0	2.88×10^{-1}	4.70×10^{-1}	1.84	3.79×10^{1}	3.20×10^{-2}
17.5	2.19	3.27	8.96×10^{-1}	2.85×10^{1}	2.82×10^{-1}
20.0	8.31×10^{-1}	1.36×10^{-2}	6.79×10^{-2}	1.09×10^{1}	2.96×10^{-1}
22.5	4.24×10^{-1}	1.00	3.12	1.79×10^{1}	9.99×10^{-1}
25.0	6.55×10^{-1}	5.77×10^{1}	4.18×10^{-1}	2.03×10^{1}	2.76×10^{-2}
27.5	1.18	2.35×10^{1}	2.37	2.74×10^{1}	1.44×10^{-1}
30.0	2.32	1.69×10^{1}	2.31	2.10×10^{1}	1.67
32.5	6.34×10^{-1}	1.73	1.40	4.29×10^{1}	2.12
35.0	1.01×10^{1}	5.42	4.48×10^{-4}	1.41×10^{2}	9.57
37.5	1.26	5.76×10^{-1}	4.09	1.49×10^{1}	1.17
40.0	6.16×10^{-1}	1.56	3.71	1.25×10^{1}	5.24×10^{-1}

Table S2 Norm N of the ground state expansion in the CDFT diabatic states for the AT-Cys, GC-Cys, CG-Cys, AT-GC and GC-CG dimers, in the selected MD snapshots of the top p53-Gadd45 DNA model system.

Time (ns)	AT-Cys	GC-Cys	CG-Cys	AT-GC	GC-CG
10.0	1.000	0.997	1.000	0.998	0.998
12.5	1.000	1.000	1.000	0.999	0.999
15.0	1.000	1.000	1.000	0.999	0.998
17.5	1.000	1.000	1.000	0.999	0.999
20.0	1.000	1.000	1.000	0.999	0.998
22.5	1.000	1.000	1.000	1.000	0.999
25.0	1.000	1.000	1.000	0.999	0.999
27.5	1.000	1.000	1.000	1.000	0.999
30.0	1.000	1.000	1.000	0.999	0.998
32.5	1.000	1.000	1.000	0.999	0.998
35.0	1.000	1.000	1.000	1.000	0.999
37.5	1.000	1.000	1.000	1.000	0.999
40.0	1.000	1.000	1.000	1.000	0.999

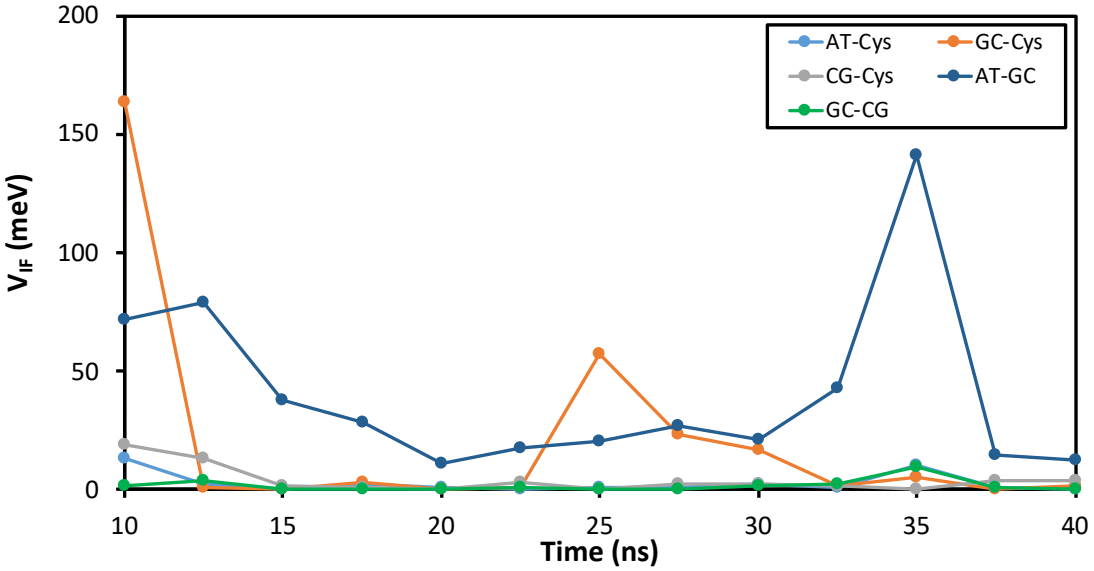

Fig. S2 Plot of V_{IF} versus MD snapshot time for the top p53-Gadd45 model system.

Table S3 V_{IF} values (in meV) for hole transfer in the AT-Cys, GC-Cys, CG-Cys, AT-GC and GC-CG dimers, in the selected MD snapshots of the bottom p53-Gadd45 DNA model system.

Time (ns)	AT-Cys	GC-Cys	CG-Cys	AT-GC	GC-CG
10.0	3.80	5.39×10^{1}	2.85×10^{1}	3.04×10^{1}	3.13×10^{-1}
12.5	8.96×10^{-1}	1.20×10^{1}	2.29×10^{1}	1.38×10^{2}	2.18×10^{-1}
15.0	1.15	1.77×10^{2}	2.81×10^{1}	1.88	7.50×10^{-2}
17.5	2.27×10^{1}	2.04×10^{2}	1.04×10^{1}	3.36×10^{1}	1.09×10^{-1}
20.0	1.69	1.22×10^{2}	1.43×10^{1}	3.25×10^{1}	1.24×10^{1}
22.5	5.55×10^{-1}	9.92×10^{1}	2.79×10^{1}	1.63×10^{1}	1.40×10^{-2}
25.0	5.92	2.88	2.14	3.19×10^{1}	3.93
27.5	1.09×10^{-2}	8.31	3.75	1.80×10^{1}	1.67
30.0	5.62	8.81×10^{-1}	1.55	6.23×10^{1}	6.44
32.5	9.14	8.33×10^{-2}	1.65	1.57×10^{2}	3.29×10^{-1}
35.0	4.27×10^{-1}	5.83×10^{-2}	3.71	1.25×10^{1}	5.24×10^{-1}
37.5	3.39×10^{-1}	1.23×10^{-2}	3.28×10^{-2}	1.55×10^{2}	5.16×10^{-1}
40.0	1.27	2.26×10^{-1}	7.91×10^{-3}	6.79×10^{1}	5.64×10^{-1}

Table S4 *N* values for the AT-Cys, GC-Cys, CG-Cys, AT-GC and GC-CG dimers, in the selected MD snapshots of the bottom p53-Gadd45 DNA model system.

Time (ns)	AT-Cys	GC-Cys	CG-Cys	AT-GC	GC-CG
10.0	1.000	0.999	0.999	1.000	0.999
12.5	1.000	1.000	1.000	0.998	0.999
15.0	1.000	0.993	1.000	0.999	0.998
17.5	1.000	0.996	1.000	1.000	0.999
20.0	1.000	0.998	1.000	0.999	0.998
22.5	1.000	0.998	1.000	0.999	0.998
25.0	1.000	1.000	1.000	0.999	0.999
27.5	1.000	1.000	1.000	0.999	0.998
30.0	1.000	1.000	1.000	0.999	0.999
32.5	1.000	1.000	1.000	0.996	0.999
35.0	1.000	1.000	1.000	0.998	0.999
37.5	1.000	1.000	1.000	0.997	0.997
40.0	1.000	1.000	1.000	1.000	0.998

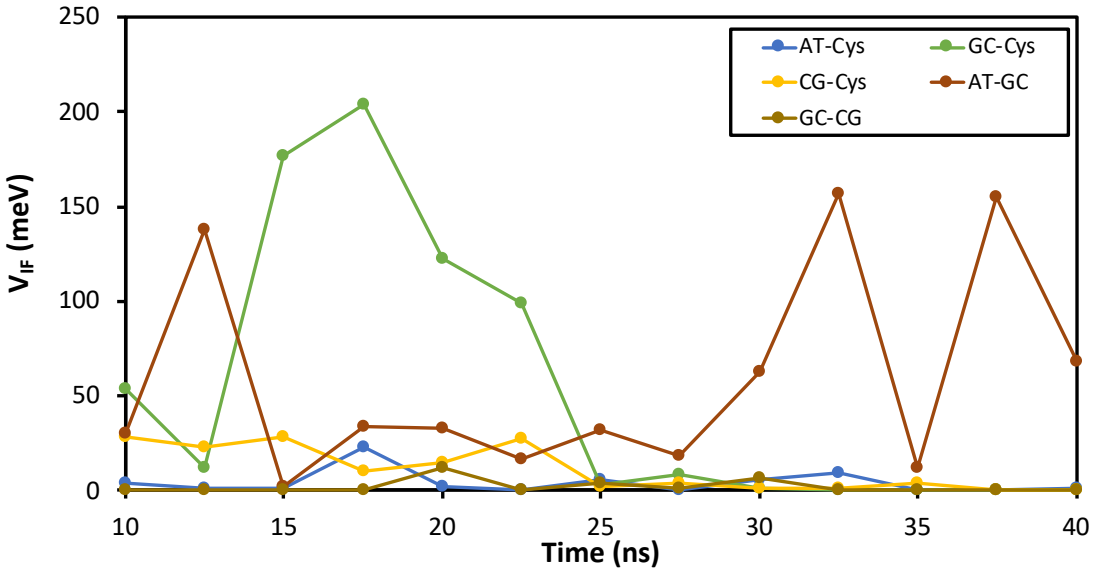

Fig. S3 Plot of V_{IF} versus MD snapshot time for the bottom p53-Gadd45 DNA model system.

Table S5 V_{IF} values (in meV) for hole transfer in the AT_1-Cys, AT_2-Cys, CG-Cys, AT_1-AT_2 and AT_2-CG dimers, in the selected MD snapshots of the top p53-p21 DNA model system.

Time (ns)	AT_1-Cys	AT_2-Cys	CG-Cys	AT_1-AT_2	AT_2-CG
10.0	2.57×10^{-1}	2.24×10^{-1}	8.11×10^{-1}	5.77×10^{1}	1.67×10^{1}
12.5	2.00	2.41×10^{-2}	5.94×10^{-1}	3.85	1.99×10^{1}
15.0	5.93×10^{-2}	1.62×10^{-1}	9.90×10^{-2}	8.98×10^{1}	2.78×10^{1}
17.5	6.27×10^{-1}	2.41×10^{-2}	9.58×10^{-2}	2.29×10^{1}	4.15
20.0	1.99	3.43×10^{-2}	3.85×10^{-1}	6.01×10^{1}	4.77
22.5	4.85×10^{-2}	8.73×10^{-3}	2.11×10^{-2}	1.89×10^{1}	4.15
25.0	3.19×10^{-1}	1.81×10^{-2}	8.99×10^{-1}	4.25	1.51×10^{1}
27.5	1.59×10^{-1}	3.19×10^{-3}	1.72	1.21×10^{1}	3.36×10^{1}
30.0	5.45×10^{-2}	2.09×10^{-3}	3.13×10^{-2}	4.70×10^{1}	1.45×10^{2}
32.5	1.10	2.47×10^{-2}	1.68	2.73×10^{1}	2.93×10^{1}
35.0	3.86×10^{-1}	3.05×10^{-3}	2.93×10^{-1}	2.25×10^{1}	2.23×10^{1}
37.5	1.99	1.83×10^{-2}	2.09×10^{-1}	2.28×10^{1}	2.46×10^{1}
40.0	4.02×10^{-1}	4.61×10^{-2}	6.80×10^{-1}	6.03×10^{1}	1.21×10^{1}

Table S6 N values for the AT_1-Cys, AT_2-Cys, CG-Cys, AT_1-AT_2 and AT_2-CG dimers, in the selected MD snapshots of the top p53-p21 DNA model system.

Time (ns)	AT_1-Cys	AT_2-Cys	CG-Cys	AT_1-AT_2	AT_2-CG
10.0	1.000	1.000	1.000	0.997	0.998
12.5	1.000	1.000	1.000	0.997	0.998
15.0	1.000	1.000	1.000	0.992	0.997
17.5	1.000	1.000	1.000	0.996	0.997
20.0	1.000	1.000	1.000	0.998	0.999
22.5	1.000	1.000	1.000	0.999	0.997
25.0	1.000	1.000	1.000	0.995	0.998
27.5	1.000	1.000	1.000	0.997	0.999
30.0	1.000	1.000	1.000	0.996	0.999
32.5	1.000	1.000	1.000	0.994	0.998
35.0	1.000	1.000	1.000	0.998	0.997
37.5	1.000	1.000	1.000	0.996	1.000
40.0	1.000	1.000	1.000	0.992	0.997

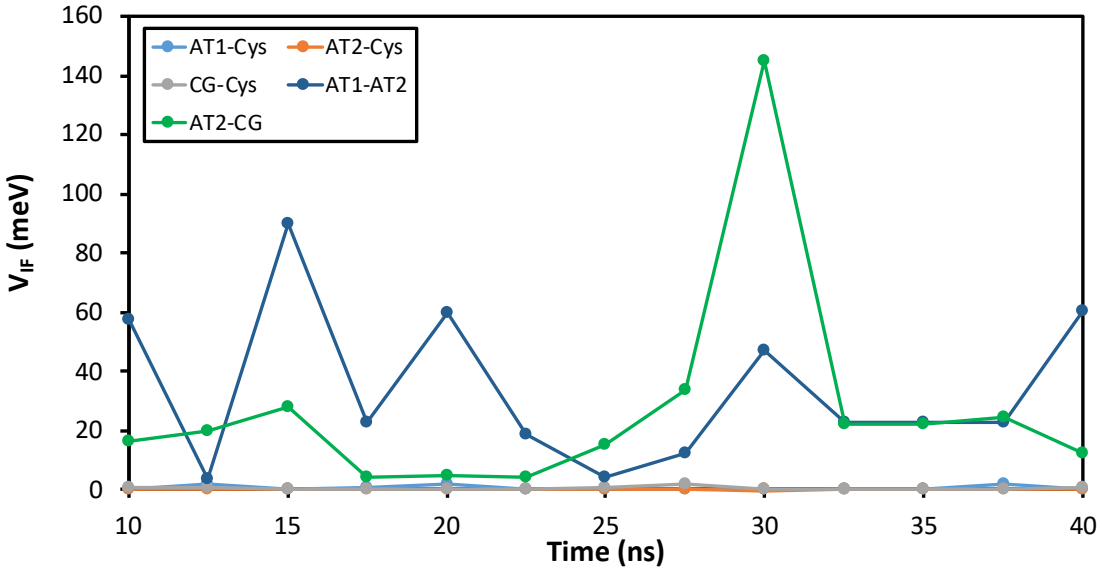

Fig. S4 Plot of V_{IF} versus MD snapshot time for the top p53-p21 DNA model system.

Table S7 V_{IF} values (in meV) for hole transfer in the AT_1-Cys, AT_2-Cys, CG-Cys, AT_1-AT_2 and AT_2-CG dimers, in the selected MD snapshots of the bottom p53-p21 DNA model system.

Time (ns)	AT_1-Cys	AT_2-Cys	CG-Cys	AT_1-AT_2	AT_2-CG
10.0	3.41×10^{-1}	5.27	5.33	2.49×10^{1}	6.98
12.5	6.45×10^{-1}	1.14	4.72	6.30	2.34×10^{1}
15.0	9.95×10^{-1}	3.50×10^{-2}	5.00×10^{-2}	7.15×10^{1}	1.14×10^{1}
17.5	9.36×10^{-1}	2.30×10^{-1}	1.61×10^{1}	1.05×10^{2}	1.63×10^{1}
20.0	8.05×10^{-1}	2.79	4.04	4.32×10^{1}	3.41
22.5	3.16×10^{-1}	2.15×10^{-1}	2.77	7.72×10^{1}	5.03
25.0	8.09×10^{-1}	2.87×10^{-2}	3.71×10^{-1}	7.09	2.53×10^{1}
27.5	1.93	4.12	3.45	6.24×10^{1}	9.33
30.0	2.32×10^{1}	9.73×10^{-1}	3.75	4.60	2.81×10^{1}
32.5	6.28×10^{-1}	1.19×10^{1}	7.53	3.03×10^{1}	9.23
35.0	2.42	1.57	3.48×10^{1}	3.68×10^{1}	8.24
37.5	1.90	3.64×10^{-1}	1.35×10^{1}	6.66×10^{1}	1.11×10^{1}
40.0	2.55×10^{-1}	1.32×10^{-2}	2.56×10^{-2}	1.89×10^{1}	1.58×10^{1}

Table S8 *N* values for the AT_1-Cys, AT_2-Cys, CG-Cys, AT_1-AT_2 and AT_2-CG dimers, in the selected MD snapshots of the bottom p53-p21 DNA model system.

Time (ns)	AT_1-Cys	AT_2-Cys	CG-Cys	AT_1-AT_2	AT_2-CG
10.0	1.000	1.000	1.000	0.995	1.000
12.5	1.000	1.000	1.000	0.996	0.999
15.0	1.000	1.000	1.000	0.995	0.998
17.5	1.000	1.000	1.000	0.996	0.996
20.0	1.000	1.000	1.000	0.997	1.000
22.5	1.000	1.000	1.000	0.998	1.000
25.0	1.000	1.000	1.000	0.999	1.000
27.5	1.000	1.000	1.000	0.999	0.998
30.0	0.999	1.000	1.000	0.995	0.996
32.5	1.000	1.000	1.000	0.994	0.997
35.0	1.000	1.000	1.000	0.997	1.000
37.5	1.000	1.000	1.000	0.993	1.000
40.0	1.000	1.000	1.000	0.993	1.000

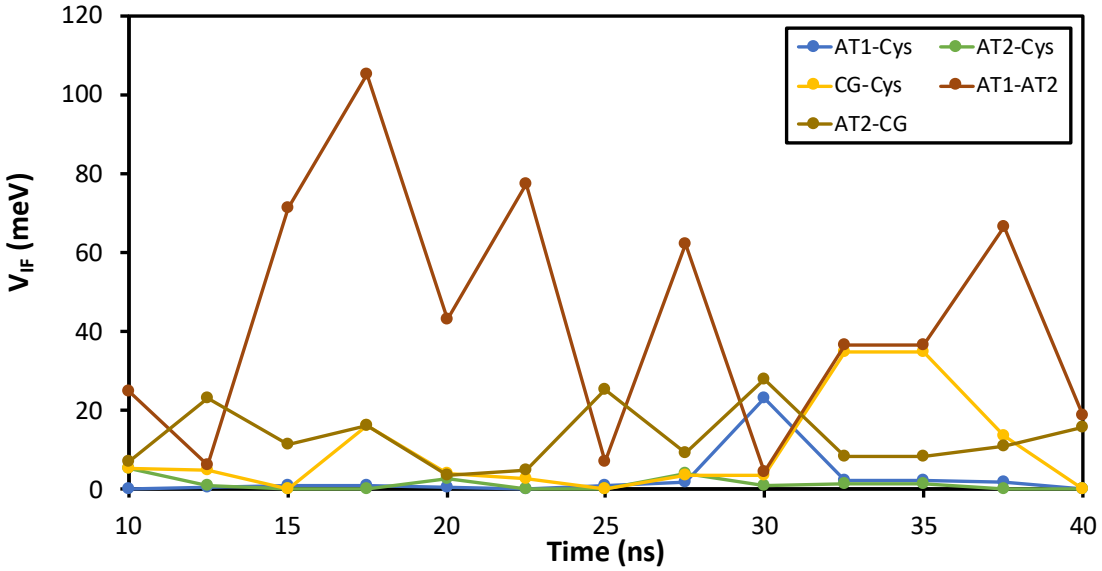

Fig. S5 Plot of V_{IF} versus MD snapshot time for the bottom p53-p21 DNA model system.

Table S9 $\langle {V_{IF}}^2 \rangle$ (meV^2), $\langle V_{IF} \rangle$ (meV) and coherence parameter $C = \langle V_{IF} \rangle^2 / \langle V_{IF}^2 \rangle$ values over the selected MD snapshots, for the indicated *D*-*A* pairs.

DNA	protein	*D*-*A* pair	$\langle {V_{IF}}^2 \rangle$	$\langle V_{IF} \rangle$	C
Gadd45 gene model	**top**	AT-Cys	2.32×10^{1}	2.79	0.34
		GC-Cys	2.39×10^{3}	2.13×10^{1}	0.19
		CG-Cys	4.56×10^{1}	4.03	0.36
		AT-GC	2.92×10^{3}	4.05×10^{1}	0.56
		GC-CG	9.16	1.73	0.33
	bottom	AT-Cys	5.30×10^{1}	4.12	0.32
		GC-Cys	7.75×10^{3}	5.24×10^{1}	0.35
		CG-Cys	2.50×10^{2}	1.11×10^{1}	0.50
		AT-GC	6.21×10^{3}	5.82×10^{1}	0.54
		GC-CG	1.64×10^{1}	2.08	0.26
p21 gene model	**top**	AT_1-Cys	1.08	7.23×10^{-1}	0.48
		AT_2-Cys	6.34×10^{-3}	4.56×10^{-2}	0.33
		CG-Cys	6.45×10^{-1}	5.79×10^{-1}	0.52
		AT_1-AT_2	1.82×10^{3}	3.46×10^{1}	0.66
		AT_2-CG	2.00×10^{3}	2.77×10^{1}	0.38
	bottom	AT_1-Cys	4.29×10^{1}	2.71	0.17
		AT_2-Cys	1.52×10^{1}	2.20	0.32
		CG-Cys	1.39×10^{2}	7.42	0.39
		AT_1-AT_2	2.75×10^{3}	4.27×10^{1}	0.66
		AT_2-CG	2.36×10^{2}	1.33×10^{1}	0.76

S3. Reorganization energies and associated parameters

Outer-sphere reorganization energy and effective radii of the G and A bases. To estimate the reorganization energies associated with the many CT processes at play, we combine Marcus theory with a DFT description of the excess charge (i.e., electron hole) localization in the *D* and *A* groups involved in the CT processes of Fig. 2. We begin our analysis with the Marcus expression for the outer-sphere contribution to the reorganization energy[24-26]

$$\lambda_{D-A}^{\text{outer-sphere}} = \left(\frac{1}{\varepsilon_o} - \frac{1}{\varepsilon_s}\right)\left(\frac{1}{2R_D} + \frac{1}{2R_A} - \frac{1}{R_{DA}}\right)(\Delta q)^2 \quad \text{(S1a)}$$

which, in the case of charge self-exchange ($D = A = X$), reduces to

$$\lambda_{X-X}^{\text{outer-sphere}} = \left(\frac{1}{\varepsilon_o} - \frac{1}{\varepsilon_s}\right)\left(\frac{1}{R_X} - \frac{1}{R_{XX}}\right)(\Delta q)^2 \quad \text{(S1b)}$$

where ε_o and ε_s denote the (relative) optical and static dielectric constants of the CT environment, respectively; Δq is the transferring charge (the elementary charge, i.e., 1 in atomic units); R_D and R_A are the effective radii of the (hole distributions on) the *D* and *A* groups, respectively, and R_{DA} is the center-to-center distance between *D* and *A*. Starting from the knowledge of the reorganization energy for the self-exchange reaction (usually given in eV, but naturally expressed in atomic units by using the equation above), one can derive the effective radius of *X* from the equation

$$R_X = 1 \Big/ \left(\lambda_{XX}^{\text{outer-sphere}} \frac{\varepsilon_s \varepsilon_o}{\varepsilon_s - \varepsilon_o} + \frac{1}{R_{XX}}\right). \quad \text{(S2)}$$

We next use the above equation to estimate the effective radii of the G and A nucleobases in DNA hole transfer (in the literature, the Marcus formula for the reorganization energy has been used to define *D* and A effective radii in virtue of its linear dependence on the inverse *D*-*A* distance;[27] see also below). To this end, we use theoretical values for the reorganization energies associated with intrastrand hole transfer between purine bases in solvated DNA, namely, $\lambda_{\text{G-G}}^{\text{outer-sphere}} = 1.41\text{eV}$ and $\lambda_{\text{A-A}}^{\text{outer-sphere}} = 1.21\,\text{eV}$,[28] and we need to make appropriate choices for the values of the average *D*-*A* distance and the dielectric constants. In fact, the $\lambda_{\text{G-G}}^{\text{outer-sphere}}$ and $\lambda_{\text{A-A}}^{\text{outer-sphere}}$ values from ref. 28 use Marcus' definition of the reorganization energy, as related to the parabolic free energy landscape, but do not make use of Marcus' formulation of the reorganization energy in terms of effective radii

and dielectric constants reported in eqn (S1b). Thus, no values are assumed or calculated for these quantities in ref. 28, but both choices influence the G and A effective radii derived from eqn (S2), which we will use to calculate the reorganization energies associated with the CT processes shown in Fig. 2.

To assess the robustness of our chemical conclusions with respect to the computational setup, we test two effective *D-A* distances: $R_{GG} = R_{AA} = 3.38$ Å and $R_{GG} = R_{AA} = 3.73$ Å. The second choice was proposed in ref. 29, using the atomic coordinates of C6, N3, C6 and N3 atoms. This choice is also consistent with the distances between adjacent purine nucleobases over the MD snapshots of our system that we obtained using all atoms, calculating their Löwdin charges and then the distance between the purine centers of charges.

Previous theoretical studies have calculated the reorganization energies dividing DNA and solvent into different dielectric zones,[27] including $\varepsilon_o = 2.27$ and $\varepsilon_s = 12.4$ for the bp stack (combined with other dielectric constants for the DNA backbone and the dielectric constants of the water solvent)[29] and values as small as 2 and 4.[30] $\varepsilon_s = 8$ was more recently found experimentally.[31] However, using the simple Marcus model of eqn (S1) requires the choice of a single set of optical and static dielectric constants. If one can make an optimal choice for these dielectric constants and for the *D-A* distance corresponding to the accurately calculated reorganization energies, the G and A effective radii that result from eqn (S2) can be approximately used as 'intrinsic' and therefore 'transferable' quantities to be inserted into eqn (S1b) to study the CT processes in the protein-DNA contact region depicted in Fig. 2. However, finding this optimal choice is out of the scope of this study. Here, we make very simple choices that consider limiting physical approximations, thus showing that our very different choices for the dielectric constants do not change our chemical-physical conclusions. We assume, first, that the effective dielectric constants in eqn (S1) are

dominated by the contribution of water, thereby using $\varepsilon_o = 1.8$ and $\varepsilon_s = 80$. Then, we also consider the opposite limit in which the intra-DNA medium provides the dominant contribution to the value of the dielectric constant, thus using $\varepsilon_o = 2.27$ and $\varepsilon_s = 12.4$,[29] as well as $\varepsilon_o = 2$[30] and $\varepsilon_s = 8$.[31] With these choices, we obtain the purine effective radii reported in Table S10, which range from a value of 1.76 Å (which is a little smaller than the value of 1.87 Å mainly used in ref. 29 for both G and A) to 2.37 Å, (which is an intermediate value compared to 1.87 Å and the value of ~ 3 Å estimated in ref. 27).

Table S10 Effective radii (in Å) of G and A as obtained from the theoretical reorganization energy values in ref. 28 using the sets of model parameters $S_1 = \{\varepsilon_o = 1.8, \varepsilon_s = 80, R_{\text{bp-bp}} = 3.38\,\text{Å}\}$, (where $R_{\text{bp-bp}}$ denotes the center-to-center base-pair distance), $S_2 = \{\varepsilon_o = 2.27, \varepsilon_s = 12.4, R_{\text{bp-bp}} = 3.38\,\text{Å}\}$, $S_3 = \{\varepsilon_o = 2, \varepsilon_s = 8, R_{\text{bp-bp}} = 3.38\,\text{Å}\}$, and the similar sets with $R_{\text{bp-bp}} = 3.73\,\text{Å}$ (that is, S_4, S_5, and S_6, respectively). We did not use a Cys effective radius to calculate the pertinent reorganization energy, but, e.g., it is $R_{\text{Cys}} = 2.14\,\text{Å}$ using the protein surface dielectric constants. The effective radii used in our analysis are in bold.

purine	S_1	S_2	S_3	S_4	S_5	S_6
G	**2.10**	**1.76**	1.80	**2.23**	**1.85**	**1.89**
A	**2.22**	**1.89**	1.92	**2.37**	**1.99**	**2.03**

We used the G and A radii in Table S10 as transferable quantities in different sets of calculations of the reorganization energies and CT rate constants, which are shown in the article and below. In contrast, to take into account the sensitivity of the R_{DA} distances involved in the CT processes of Fig. 2 to structural fluctuations, we calculated by using DFT the conformation-dependent *D* and *A* centers of charge for each CT process as detailed in the next subsection.

Calculation of R_{DA}. Since the transferring hole essentially localizes in purine nucleobases, because of their lower oxidation potentials than pyrimidines,[32, 33] the centers of the charge localizations in G and A are good approximations to those for the G-C or A-T bps. For each selected MD snapshot, we pruned the CT model systems in Fig. 2, saturated the dangling bonds with H atoms, and optimized the positions of the latter in each redox-active moiety (with the charge in it) individually, at the B3LYP/6-31g* level of DFT approximation, with the Grimme's DFT-D3 correction for the dispersion energy terms.[34] In addition to using the optimized geometries for V_{IF} calculations, we derived the Löwdin net charges on the atoms of G, A, and Cys (for each selected structure snapshot) from the DFT Löwdin spin densities and calculated the positions of the pertinent centers of charge using the standard formula $\mathbf{r}_c = \sum_i q_i \mathbf{r}_i$, where the summation runs over the atoms of a given group, q_i is the Löwdin charge of atom i, and $\mathbf{r}_i$ is its position vector. The coordinates and Löwdin charges of the three redox-active groups in the first MD snapshot, at 10 ns, are reported in Tables S11-S14 as an example. The center-to-center distance R_{DA} of a *D*-*A* pair for a given MD snapshot was then obtained from *D* and *A* coordinates (Tables S15-S18).

Table S11 Atomic coordinates and Löwdin charges (in units of elementary charge) of the pruned C277 cation in the top p53 protein complexed with the model Gadd45 DNA sequence, in the first selected snapshot (at 10 ns of MD production run). This is the Cys in the model system of Fig. 2.

atom	*X*	*Y*	*Z*	*q*
H	42.0176	31.8788	39.8335	0.0281
C	42.7840	31.1670	40.1500	0.0016
H	42.7160	31.0610	41.2470	-0.0004
H	42.7080	30.2550	39.5670	0.0345
S	44.4740	31.8580	39.8110	0.9547
H	44.2620	32.1160	38.5150	-0.0186

Table S12 Atomic coordinates and Löwdin charges of the A nucleobase in the model CT system of Fig. 2 (complex and snapshot are the same as in Table S11).

atom	*X*	*Y*	*Z*	*q*
H	50.5288	24.0867	37.7802	-0.0006
N	49.8770	24.8580	37.8290	0.0121
C	48.5640	24.8080	38.1040	0.1236
H	48.0170	23.8800	38.4040	-0.0044
N	47.9750	26.0100	37.9930	0.0789
C	49.0000	26.8820	37.6950	0.1399
C	49.1330	28.2270	37.3200	0.0319
N	48.1550	29.1120	37.3130	0.3115
H	48.3250	30.0570	37.0600	-0.0064
H	47.2390	28.7130	37.0800	-0.0056
N	50.2980	28.8290	37.1670	0.0592
C	51.3490	28.0750	37.1220	0.0166
H	52.3000	28.6130	36.8600	-0.0013
N	51.4200	26.7320	37.2720	0.2508
C	50.1890	26.1540	37.5590	-0.0062

Table S13 Atomic coordinates and Löwdin charges for the G base of the GC bp in the model CT system of Fig. 2 (complex and snapshot are the same as in Table S11).

atom	*X*	*Y*	*Z*	*q*
H	53.2141	27.0253	40.4176	0.0004
N	52.2640	27.3310	40.5770	-0.0336
C	51.1990	26.5940	41.1430	0.2331
H	51.1740	25.5140	41.3410	-0.0077
N	50.0900	27.2900	41.0770	-0.0235
C	50.4560	28.5530	40.5970	0.2839
C	49.7860	29.8290	40.1670	-0.0546
O	48.5750	29.9820	40.0880	0.1785
N	50.6140	30.8680	39.8010	-0.0082
H	50.2660	31.7340	39.7440	-0.0003
C	51.9280	30.6830	39.5740	0.0098
N	52.6410	31.7900	39.5170	0.1271
H	52.2550	32.7100	39.6800	-0.0035
H	53.6080	31.6940	39.6590	-0.0025
N	52.5920	29.6110	39.8400	0.2307
C	51.7880	28.5780	40.2980	0.0705

Table S14 Atomic coordinates and Löwdin charges for the G base of the CG bp in the model CT system of Fig. 2 (complex and snapshot are the same as in Table S11).

atom	*X*	*Y*	*Z*	*q*
H	47.2713	38.0809	43.1230	0.0001
N	47.1890	37.0910	42.9260	-0.0207
C	46.1370	36.3060	43.2530	0.2457
H	45.1230	36.6670	43.2410	-0.0065
N	46.3860	34.9890	43.1810	0.0315
C	47.7180	34.9490	43.0020	0.2248
C	48.5820	33.7900	43.0580	-0.0290
O	48.4040	32.6340	43.2750	0.1224
N	49.8860	34.1870	42.9360	-0.0138
H	50.5950	33.5040	42.9680	0.0000
C	50.3430	35.4760	42.9480	0.0177
N	51.5740	35.5970	42.6250	0.1205
H	52.1340	34.7540	42.4990	-0.0034
H	51.8810	36.5770	42.4450	-0.0033
N	49.6030	36.5520	42.9120	0.2218
C	48.2980	36.1990	42.9600	0.0923

Table S15 R_{DA} (in Å) for the indicated redox pairs in the selected MD structure snapshots of the top p53 protein - Gadd45 DNA complex.

Time (ns)	**AT-Cys**	**GC-Cys**	**CG-Cys**	**AT-GC**	**GC-CG**
10.0	7.08	7.36	6.32	3.72	7.63
12.5	7.85	7.77	7.62	3.57	6.44
15.0	7.90	9.29	8.76	3.74	7.62
17.5	7.56	8.71	8.82	3.86	7.18
20.0	8.53	9.58	9.69	3.47	7.22
22.5	7.72	8.64	8.62	3.72	7.24
25.0	8.02	8.30	8.92	3.78	7.61
27.5	7.68	8.11	8.79	4.06	7.54
30.0	7.03	8.19	8.75	3.80	7.24
32.5	7.45	8.94	8.88	3.57	6.92
35.0	7.42	7.93	7.89	3.74	7.99
37.5	7.91	9.37	8.62	4.25	7.92
40.0	7.65	8.01	8.61	3.80	7.81

Table S16 R_{DA} (in Å) for the indicated redox pairs in the selected MD structure snapshots of the bottom p53-Gadd45 DNA complex.

Time (ns)	AT-Cys	GC-Cys	CG-Cys	AT-GC	GC-CG
10.0	7.45	6.67	6.40	3.72	7.21
12.5	7.07	6.57	6.39	3.54	6.56
15.0	7.99	7.62	6.08	3.54	7.29
17.5	6.28	7.84	6.42	4.29	7.64
20.0	7.24	7.11	6.24	3.91	6.59
22.5	8.88	8.38	6.24	3.86	7.30
25.0	6.77	8.05	8.72	3.44	6.92
27.5	7.54	6.76	8.37	3.80	6.77
30.0	6.63	7.74	8.70	3.67	6.58
32.5	6.85	8.26	9.16	3.50	6.20
35.0	7.62	9.46	10.12	3.49	6.32
37.5	7.79	8.72	9.92	3.35	6.30
40.0	7.58	9.12	10.69	3.74	6.12

Table S17 R_{DA} (in Å) for the indicated redox pairs in the selected MD structure snapshots of the top p53–p21 DNA complex.

Time (ns)	AT_1-Cys	AT_2-Cys	CG-Cys	AT_1-AT_2	AT_2-CG
10.0	8.34	9.33	9.21	3.54	6.54
12.5	7.77	9.97	9.39	3.64	6.37
15.0	8.30	9.29	9.05	3.40	6.43
17.5	8.17	9.58	9.33	3.66	6.91
20.0	7.37	9.97	9.11	4.17	6.72
22.5	8.54	10.09	9.12	3.58	6.52
25.0	8.91	9.47	8.85	3.51	6.88
27.5	8.73	10.44	8.89	3.92	5.95
30.0	8.77	11.36	10.28	4.13	6.47
32.5	7.40	9.66	8.95	4.09	6.47
35.0	9.34	11.66	9.95	3.99	6.91
37.5	8.04	10.26	8.50	4.19	6.33
40.0	8.06	9.71	9.18	3.61	6.68

Table S18 R_{DA} (in Å) for the indicated redox pairs in the selected MD structure snapshots of the bottom p53–p21 DNA complex.

Time (ns)	AT_1-Cys	AT_2-Cys	CG-Cys	AT_1-AT_2	AT_2-CG
10.0	7.07	8.22	8.12	3.66	6.92
12.5	8.20	8.43	7.87	3.54	6.54
15.0	7.84	9.81	9.61	3.40	6.70
17.5	7.65	8.46	7.50	3.34	6.51
20.0	8.05	8.83	8.22	3.49	7.05
22.5	8.20	9.07	8.30	3.76	6.66
25.0	7.98	9.38	7.72	4.05	6.65
27.5	7.40	8.73	8.49	3.64	6.85
30.0	5.70	7.80	6.57	3.82	6.66
32.5	6.78	7.55	6.61	3.58	6.25
35.0	6.61	8.08	5.73	4.01	6.76
37.5	7.29	8.42	6.13	3.41	6.61
40.0	8.43	9.82	9.46	4.19	6.56

Calculation of λ. To estimate the reorganization energies, we make use of a further approximation in the Marcus theory. Given two redox species 1 and 2 that can be oxidized (Ox) or reduced (Red), the reorganization energies λ_{11} and λ_{22} associated with the weak-overlap self-exchange reactions

$$\mathrm{Ox}_n + \mathrm{Red}_n \rightleftharpoons \mathrm{Red}_n + \mathrm{Ox}_n \quad (n = 1, 2) \tag{S3}$$

can be related to the reorganization energy λ for the cross-reaction

$$\mathrm{Ox}_1 + \mathrm{Red}_2 \rightleftharpoons \mathrm{Red}_1 + \mathrm{Ox}_2 \tag{S4}$$

by the approximate relationship[35-37]

$$\lambda = \frac{\lambda_{11} + \lambda_{22}}{2} \equiv \lambda_1 + \lambda_2 \tag{S5}$$

where the contribution of each redox species to the reorganization energy of the cross-reaction is

given by half the reorganization energy for the self-exchange reaction:

$$\lambda_n \equiv \frac{\lambda_{nn}}{2} \qquad (n = 1, 2)\,. \tag{S6}$$

The total reorganization energy contains the inner-sphere and outer-sphere contributions.[25] For the A and G nucleobases, we used the inner-sphere reorganization energies $\lambda_{\mathrm{G-G}}^{\mathrm{inner-sphere}} = 0.746$ eV and $\lambda_{\mathrm{A-A}}^{\mathrm{inner-sphere}} = 0.423$ eV.[38] The purine contributions to the reorganization energies (λ_{X}, X = G, A) for the CT processes at the protein-DNA interface were then obtained from the equation

$$\lambda_X = \frac{1}{2}\lambda_{X-X}^{\mathrm{inner-sphere}} + \frac{1}{2}\left(\frac{1}{\varepsilon_o} - \frac{1}{\varepsilon_s}\right)\left(\frac{1}{R_X} - \frac{1}{R_{XX}}\right)(\Delta q)^2 \qquad (X = \mathrm{G, A}) \tag{S7}$$

using the different sets of R_X (X = G, A) values in Table S10 and dielectric constants that describe the CT environment at the protein-DNA interface (see below). Eqn (S7) aims to maximize the use of the accurate computational values for the reorganization energies given in ref. 28, while limiting to the $1/R_{XX}$ term the changes due to the fluctuating *D-A* distances during the motion of the p53-DNA complex. To apply eqn (S7) to the CT processes of Fig. 2 in different MD snapshots, we set R_{XX} to the pertinent R_{DA} value reported in one of Tables S15-S18. Alternatively, one can estimate the effective radii of G and A from the atomic Löwdin charges, but this choice would not allow us to use the knowledge of previous accurate calculations of the reorganization energies for the G-G and A-A pairs.[28]

Next, before considering the contribution to the reorganization energies of the Cys moiety (λ_{Cys}), we discuss the dielectric constants to be used in the description of the CT processes at the protein-DNA interface and thus, in particular, in eqn (S7). A very simple choice consists in assuming that the protein surrounding the contact with DNA mostly determines the dielectric constants required

to describe the CT processes in Fig. 2 by means of Marcus' expression for the outer-sphere reorganization energy. In this physical limit, we use $\varepsilon_o = 2.2$ [39] and $\varepsilon_s = 4.0$.[40] Another limiting case is that the effective dielectric constants are determined by protein and water, and the DNA sequence does not change appreciably their values. A recent study shows a significant increase in ε_s proceeding from the inner part of a globular protein to its surface, where more polar or charge residues are in contact with water, and ε_s is located in the range 20 to 30 for the protein surface.[41] In this perspective, we use $\varepsilon_s = 25$, which is still much lower than the value for water, but much larger than the value in the hydrophobic core of a protein. Ref. 41 does not provide a value for ε_o. For simplicity, we assume a similar and linear scaling of the two dielectric constants with the proximity to the surface and the percentage of surrounding water, thus obtaining $\varepsilon_o = 2.1$. The two very different dielectric constant sets $\{\varepsilon_o = 2.1, \varepsilon_s = 25\}$ and $\{\varepsilon_o = 2.2, \varepsilon_s = 4\}$ lead to the same conclusions on interfacial charge dynamics discussed in the article (cf. Table S19 with Tables S20-S22). These two sets of relative dielectric constants enclose the values discussed above for the DNA medium. Therefore, considering the effects of the latter would again not change the conclusions described in the article.

To calculate λ_{Cys}, we make use of the reorganization energies that were obtained in ref. 42 for hole transfer through polyproline II helices at an average donor-acceptor distance $\bar{R}_{DA} = 12.8$ Å. For this system, we can use again the two sets $\{\varepsilon_o = 2.1, \varepsilon_s = 25\}$ and $\{\varepsilon_o = 2.2, \varepsilon_s = 4\}$. We expect that the first set is the most suitable one for this case because the helix is surrounded by water. Nonetheless, we also use the second set of values, in combination with the same choice for the p53-DNA contact region, to test further the robustness of our chemical conclusions. Differently from the case of the DNA purines, since we associate the same dielectric constants to the hole

transfer processes at the p53-DNA interface and in ref. 42, we do not need to use Cys effective radii and we can instead proceed as follows.

Ref. 42 provides the reorganization energy values $\lambda_{\mathrm{Tyr-Tyr}} = 2.04\,\mathrm{eV}$ and $\lambda_{\mathrm{Tyr-Cys}} = 2.29\,\mathrm{eV}$. At the same donor-acceptor distance $\bar{R}_{DA} = 12.8\,\text{Å}$, eqn (S6) implies $\lambda_{\mathrm{Tyr}} = 1.02$, and then eqn (S5) gives $\lambda_{\mathrm{Cys}}(\bar{R}_{DA}) = \lambda_{\mathrm{Tyr-Cys}} - \lambda_{\mathrm{Tyr}} = 1.27\,\mathrm{eV}$, namely, $\lambda_{\mathrm{Cys-Cys}}(\bar{R}_{DA}) = 2.54\,\mathrm{eV}$ (here, we indicated explicitly the specific *D-A* distance corresponding to these reorganization energies). To get the reorganization energy for a self-exchange reaction at a distance $R_{DA} \neq \bar{R}_{DA} = 12.8\,\text{Å}$ (which will be the distance at which we need to compute the contribution of Cys to the reorganization energy for the actual cross-reaction with a bp), we use eqn (S1b) for the outer-sphere component of the reorganization energy and we also assume that the inner-sphere component of $\lambda_{\mathrm{Cys-Cys}}$ and the effective radius of the Cys moiety are approximately independent of the Cys-Cys distance. The second approximation implies that we can calculate λ_{Cys}, without knowing the radius of the Cys moiety, as

$$\lambda_{\mathrm{Cys}} = \frac{1}{2}\lambda_{\mathrm{Cys-Cys}}(\bar{R}_{DA}) + \frac{1}{2}\left(\frac{1}{\varepsilon_o} - \frac{1}{\varepsilon_s}\right)(\Delta q)^2\left(\frac{1}{\bar{R}_{DA}} - \frac{1}{R_{DA}}\right). \qquad \text{(S8)}$$

The use of eqn (S8) is supported by previous theoretical studies that showed the approximate linear dependence of the reorganization energy on the inverse *D-A* distance[27, 43] predicted by the Marcus model. Importantly, the approach described by eqn (S8) combines this useful characteristic of the Marcus formula with the value of the reorganization energy derived from the accurate calculations of ref. 42. The quality of the approximations inherent in the above equation is further improved by the fact that all Cys-bp center-to-center distances in the p53-DNA complexes studied here (Tables S15-S18) are significantly larger than the effective radius of Cys.

Since the reorganization energy is a free energy quantity and the molecular complex is equilibrated throughout the MD run from which the structure snapshots were drawn, the 'instantaneous' values obtained using eqns (S7) and (S8) are averaged over the snapshots to obtain the reorganization energies in Tables S19-S23, which enter the Marcus expression for the hole transfer rate constants.

S4. Charge-transfer parameters and rate constants using different base-pair spacing and dielectric constants

In this section, we present the values of CT parameters and rate constants obtained using the sets of model parameters in Table S10 and employing the sets of dielectric constants $\{\varepsilon_o = 2.2, \varepsilon_s = 4\}$ or $\{\varepsilon_o = 2.1, \varepsilon_s = 25\}$ to describe the p53-DNA interface. To calculate the CT rates, we estimated the reaction free energies ΔG^0 associated with the CT processes using the experimental oxidation potential values for Cys (0.92[44]), G (1.29[45, 46]), and A (1.42[45]). The resulting CT rates are reported in Table S19-S23 and illustrated in Fig. 2 and Fig. S6-S9. In Tables S19-S23 we also report the rates for back hole transfer from Cys to DNA. These rates are much smaller than the converse CT rates and allow the Cys to depart from the DNA before giving the charge back.

Table S19 presents the results illustrated in Fig. 2 of the article, which correspond to the following (simplest) modeling choices. The effective radii of the purine nucleobases were extracted from the computed outer-sphere reorganization energy values in ref. 28, by assuming that the water solvent dominated these values and that the effective distance between adjacent purine nucleobases on the same strand was 3.73 Å, that is, the model parameter set $S_4 = \{\varepsilon_o = 1.8, \varepsilon_s = 80, R_{\text{bp-bp}} = 3.73\,\text{Å}\}$ was used. The other simple first choice was to use common values of the dielectric constants for protein matrices, $\varepsilon_o = 2.2$ and $\varepsilon_s = 4$, thus assuming that the CT processes between the Cys residue and

the bps within the contact region is dominated by the surrounding protein.

The robustness of our conclusions with respect to the modeling was first tested with respect to the bp-bp distance, using the above parameter set except for $R_{\mathrm{bp-bp}} = 3.38\,\text{Å}$. This is a "naïve" choice, yet it approximately amounts to a zero-order physical description in which the transferring electron hole is uniformly distributed over purine atoms. The CT results making use of this choice are listed in Table S20 and shown in Fig. S6.

Table S21 and Fig. S7 use $\mathcal{S}_5 = \left\{\varepsilon_o = 2.27, \varepsilon_s = 12.4, R_{\mathrm{bp-bp}} = 3.73\,\text{Å}\right\}$ to obtain the purine effective radii and dielectric constants typical of a protein surface exposed to water ($\varepsilon_o = 2.1$ and $\varepsilon_s = 25$) to compute the CT rate constants. These two dielectric constants are also used to describe the p53-DNA contact region in Table S22, Fig. S8 and Table S23, Fig. S9, where the purine nucleobase effective radii result from using $\mathcal{S}_2 = \left\{\varepsilon_o = 2.27, \varepsilon_s = 12.4, R_{\mathrm{bp-bp}} = 3.38\,\text{Å}\right\}$ and $\mathcal{S}_6 = \left\{\varepsilon_o = 2, \varepsilon_s = 8, R_{\mathrm{bp-bp}} = 3.73\,\text{Å}\right\}$, respectively. Note that the choices of model physical parameters that produce the smallest effective radii of the G and A nucleobases also lead to the largest reorganization energy values, which may turn out to be exceedingly large but, even more, confirm the validity of our conclusions irrespective of more accurate determinations of the physical parameters describing the protein-DNA sequence contact region.

While the above choices do not exhaust all possible combinations of parameters, they all share the main characteristics of the charge dynamics at the p53-DNA interface that distinguish the Gadd45 and p21 sequences: the GC pair can more easily release the charge to Cys and more slowly transfer it to the next CG pair, compared to AT_2. Both differences in CT rates, and their interplay, are important to determine the different behaviors of the two protein-DNA complexes under oxidative stress.

Table S19 Protein gene (Gadd45 or p21) corresponding to the model DNA sequence used, protein location, redox pair, average *D-A* distance over the selected MD snapshots ($\langle R_{DA} \rangle$), reorganization energy (λ), reaction free energy ΔG^0, forward (k_f) and backward (k_b) hole transfer rate constant, as obtained by using the parameter set $S_4 = \{\varepsilon_o = 1.8, \varepsilon_s = 80, R_{\text{bp-bp}} = 3.73\,\text{Å}\}$ to derive the effective radii of G and A and $\varepsilon_o = 2.2$, $\varepsilon_s = 4$ to describe the CT processes at the protein-DNA interface.

DNA	protein	D-A pair	$\langle R_{DA} \rangle$ (Å)	λ (eV)	$\Delta G°$ (eV)	k_f (s^{-1})	k_b (s^{-1})
Gadd45 gene model	Top	AT-Cys	7.68	1.83	-0.50	2.29×10^{7}	8.01×10^{-2}
		GC-Cys	8.48	2.07	-0.37	3.53×10^{7}	1.95×10^{1}
		CG-Cys	8.48	2.07	-0.37	6.81×10^{5}	3.77×10^{-1}
		AT-GC	3.78	1.08	-0.13	1.32×10^{10}	8.38×10^{7}
		GC-CG	7.41	1.67	0.00	1.06×10^{4}	1.06×10^{4}
	Bottom	AT-Cys	7.36	1.81	-0.50	6.21×10^{7}	2.17×10^{-1}
		GC-Cys	7.87	2.04	-0.37	1.52×10^{8}	8.41×10^{1}
		CG-Cys	7.96	2.03	-0.37	5.26×10^{6}	2.91
		AT-GC	3.68	1.06	-0.13	3.51×10^{10}	2.22×10^{8}
		GC-CG	6.75	1.63	0.00	2.81×10^{4}	2.81×10^{4}
p21 gene model	Top	AT_1-Cys	8.29	1.86	-0.50	8.25×10^{5}	2.89×10^{-3}
		AT_2-Cys	10.06	1.92	-0.50	2.69×10^{3}	9.41×10^{-6}
		CG-Cys	9.21	2.10	-0.37	7.17×10^{3}	3.97×10^{-3}
		AT_1-AT_2	3.80	0.89	0.00	5.78×10^{9}	5.78×10^{9}
		AT_2-CG	6.55	1.42	-0.13	3.26×10^{8}	2.06×10^{6}
	Bottom	AT_1-Cys	7.48	1.82	-0.50	4.81×10^{7}	1.68×10^{-1}
		AT_2-Cys	8.66	1.88	-0.50	1.01×10^{7}	3.54×10^{-2}
		CG-Cys	7.72	2.03	-0.37	3.06×10^{6}	1.69
		AT_1-AT_2	3.68	0.86	0.00	1.12×10^{10}	1.12×10^{10}
		AT_2-CG	6.67	1.42	-0.13	3.53×10^{7}	2.24×10^{5}

Table S20 Same properties as in Table 20. The parameters $\mathcal{S}_1 = \{\varepsilon_o = 1.8, \varepsilon_s = 80, R_{\text{bp-bp}} = 3.38\,\text{Å}\}$ were used to obtain the purine effective radii; the dielectric constants $\varepsilon_o = 2.2$ and $\varepsilon_s = 4$ describe the p53-DNA interface.

DNA	protein	D-A pair	$\langle R_{DA} \rangle$ (Å)	λ (eV)	$\Delta G°$ (eV)	k_f (s^{-1})	k_b (s^{-1})
Gadd45 gene model	Top	AT-Cys	7.68	1.88	-0.50	1.55×10^{7}	5.42×10^{-2}
		GC-Cys	8.48	2.11	-0.37	2.38×10^{7}	1.31×10^{1}
		CG-Cys	8.48	2.11	-0.37	4.59×10^{5}	2.54×10^{-1}
		AT-GC	3.78	1.17	-0.13	5.75×10^{9}	3.64×10^{7}
		GC-CG	7.41	1.75	0.00	4.65×10^{3}	4.65×10^{3}
	Bottom	AT-Cys	7.36	1.86	-0.50	4.20×10^{7}	1.47×10^{-1}
		GC-Cys	7.87	2.08	-0.37	1.03×10^{8}	5.67×10^{1}
		CG-Cys	7.96	2.07	-0.37	3.54×10^{6}	1.96
		AT-GC	3.68	1.15	-0.13	1.53×10^{10}	9.66×10^{7}
		GC-CG	6.75	1.71	0.00	1.24×10^{4}	1.24×10^{4}
p21 gene model	Top	AT_1-Cys	8.29	1.90	-0.50	5.58×10^{5}	1.95×10^{-3}
		AT_2-Cys	10.06	1.97	-0.50	1.82×10^{3}	6.36×10^{-6}
		CG-Cys	9.21	2.14	-0.37	4.83×10^{3}	2.67×10^{-3}
		AT_1-AT_2	3.80	0.97	0.00	2.44×10^{9}	2.44×10^{9}
		AT_2-CG	6.55	1.50	-0.13	1.42×10^{8}	9.01×10^{5}
	Bottom	AT_1-Cys	7.48	1.86	-0.50	3.25×10^{7}	1.14×10^{-1}
		AT_2-Cys	8.66	1.92	-0.50	6.84×10^{6}	2.39×10^{-2}
		CG-Cys	7.72	2.07	-0.37	2.06×10^{6}	1.14
		AT_1-AT_2	3.68	0.95	0.00	4.73×10^{9}	4.73×10^{9}
		AT_2-CG	6.67	1.51	-0.13	1.54×10^{7}	9.77×10^{4}

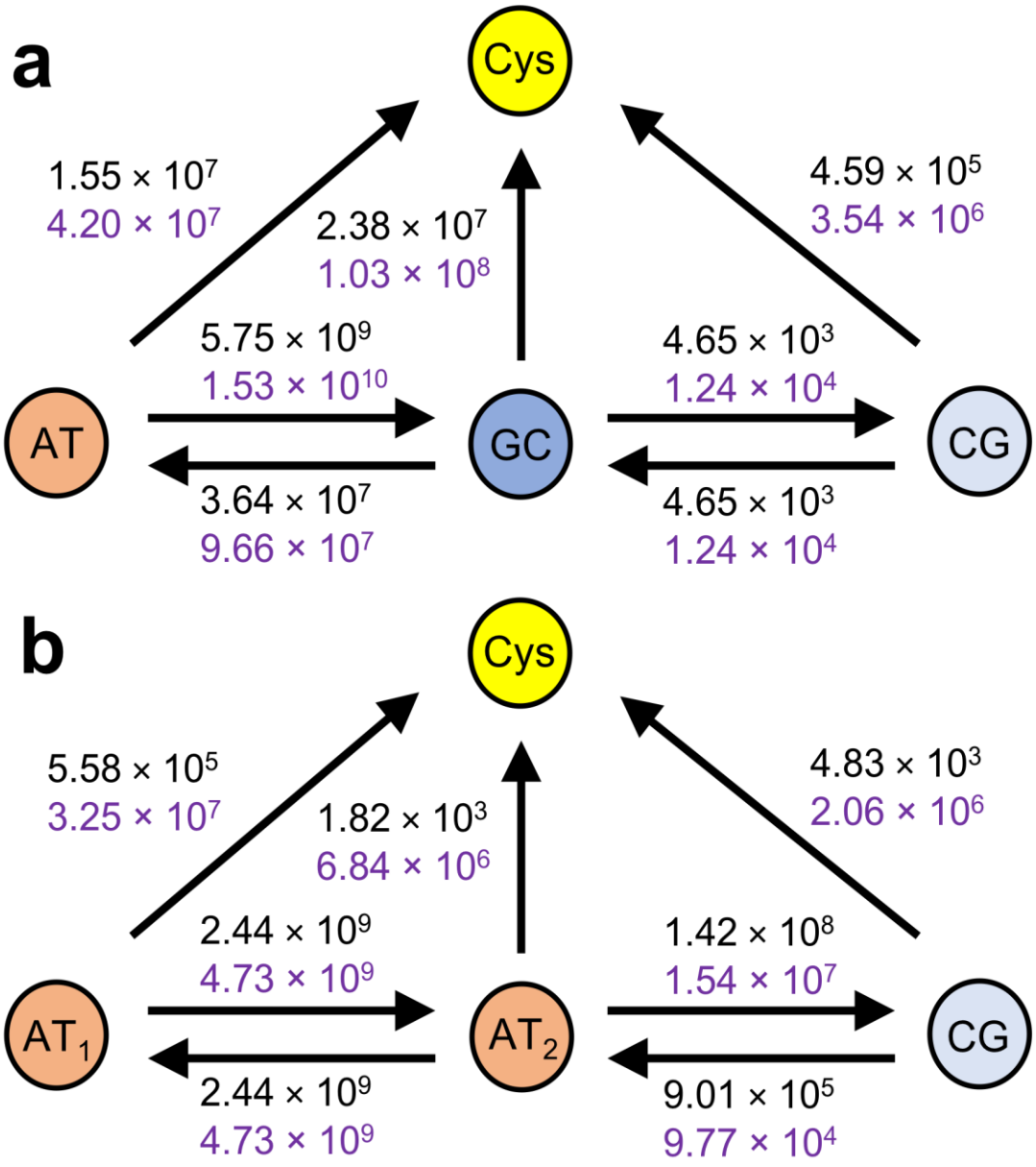

Fig. S6 The CT model systems for the p53-DNA contact region are represented as in Fig. 2 of the article. The value of the hole-transfer rate constants (in s^{-1}) are reported from Table S20.

Table S21 Same properties as in Table 20. $S_5 = \{\varepsilon_o = 2.27, \varepsilon_s = 12.4, R_{\text{bp-bp}} = 3.73\,\text{Å}\}$ was used to obtain the purine effective radii; the dielectric constants $\varepsilon_o = 2.1$ and $\varepsilon_s = 25$ described the p53-DNA interface.

DNA	protein	D-A pair	$\langle R_{DA} \rangle$ (Å)	λ (eV)	$\Delta G°$ (eV)	k_f (s^{-1})	k_b (s^{-1})
Gadd45 gene model	Top	AT-Cys	7.68	2.48	-0.50	4.90×10^{4}	1.71×10^{-4}
		GC-Cys	8.48	2.84	-0.37	1.96×10^{4}	1.08×10^{-2}
		CG-Cys	8.48	2.84	-0.37	3.84×10^{2}	2.12×10^{-4}
		AT-GC	3.78	2.19	-0.13	2.07×10^{5}	1.31×10^{3}
		GC-CG	7.41	3.29	0.00	1.03×10^{-3}	1.03×10^{-3}
	Bottom	AT-Cys	7.36	2.45	-0.50	1.63×10^{5}	5.71×10^{-4}
		GC-Cys	7.87	2.78	-0.37	1.18×10^{5}	6.50×10^{-2}
		CG-Cys	7.96	2.76	-0.37	4.40×10^{3}	2.43×10^{-3}
		AT-GC	3.68	2.15	-0.13	7.00×10^{5}	4.43×10^{3}
		GC-CG	6.75	3.21	0.00	4.27×10^{-3}	4.27×10^{-3}
p21 gene model	Top	AT_1-Cys	8.29	2.54	-0.50	1.30×10^{3}	4.56×10^{-6}
		AT_2-Cys	10.06	2.68	-0.50	2.11	7.39×10^{-9}
		CG-Cys	9.21	2.90	-0.37	2.88	1.59×10^{-6}
		AT_1-AT_2	3.80	1.92	0.00	1.71×10^{5}	1.71×10^{5}
		AT_2-CG	6.55	2.90	-0.13	1.28×10^{2}	8.13×10^{-1}
	Bottom	AT_1-Cys	7.48	2.46	-0.50	1.20×10^{5}	4.19×10^{-4}
		AT_2-Cys	8.66	2.58	-0.50	1.35×10^{4}	4.73×10^{-5}
		CG-Cys	7.72	2.75	-0.37	2.69×10^{3}	1.48×10^{-3}
		AT_1-AT_2	3.68	1.87	0.00	4.35×10^{5}	4.35×10^{5}
		AT_2-CG	6.67	2.92	-0.13	1.27×10^{1}	8.05×10^{-2}

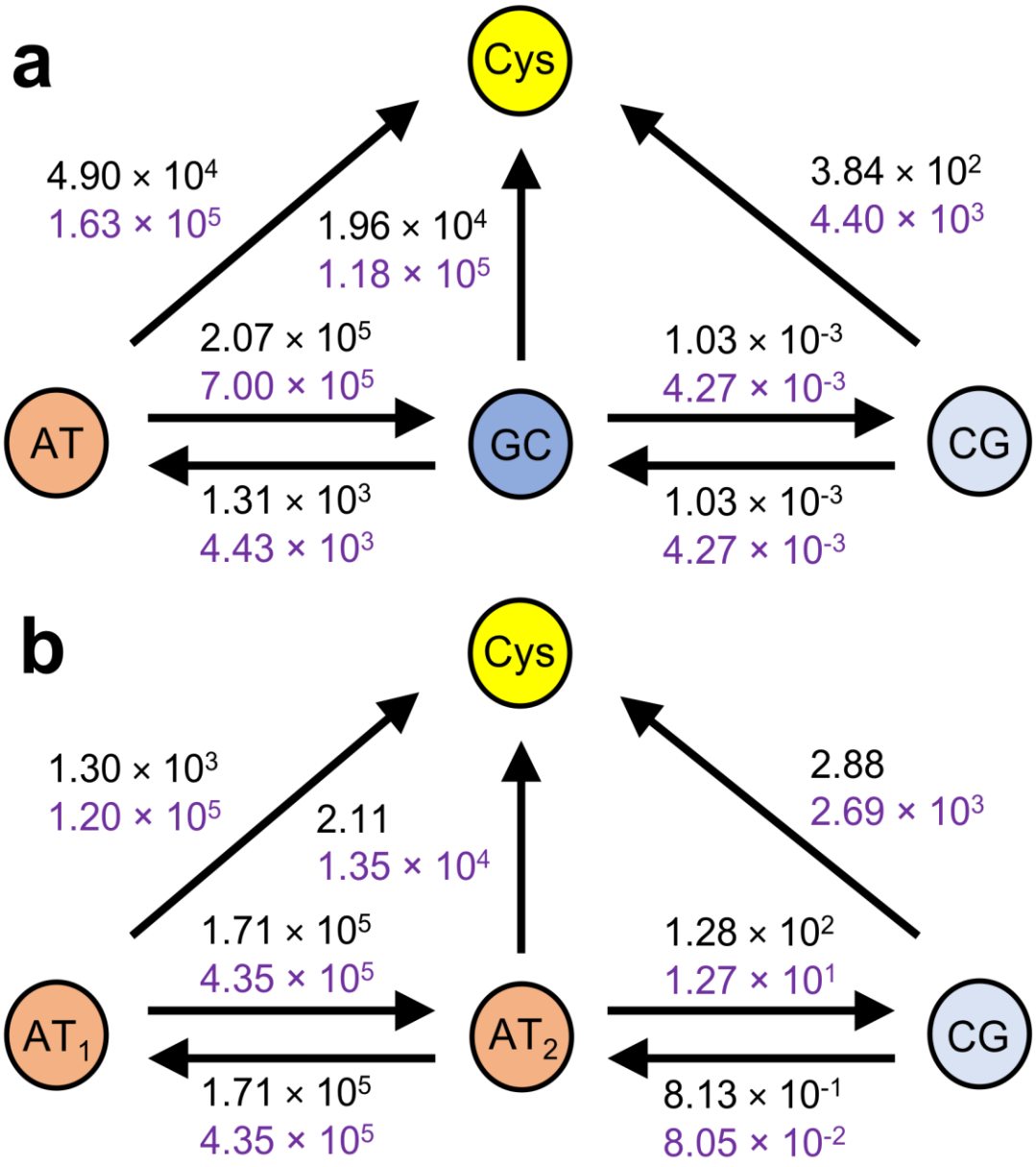

Fig. S7 The CT model systems for the p53-DNA contact region are represented as in Fig. 2 of the article. The value of the hole-transfer rate constants (in s^{-1}) are reported from Table S21.

Table S22 Same properties as in Table 20. $S_5 = \{\varepsilon_o = 2.27, \varepsilon_s = 12.4, R_{\text{bp-bp}} = 3.38\,\text{Å}\}$ was used to obtain the purine effective radii; the dielectric constants $\varepsilon_o = 2.1$ and $\varepsilon_s = 25$ described the p53-DNA interface.

DNA	protein	D-A pair	$\langle R_{DA} \rangle$ (Å)	λ (eV)	$\Delta G°$ (eV)	k_f (s^{-1})	k_b (s^{-1})
Gadd45 gene model	Top	AT-Cys	7.68	2.51	-0.50	4.01×10^{4}	1.40×10^{-4}
		GC-Cys	8.48	2.93	-0.37	8.41×10^{3}	4.65×10^{-3}
		CG-Cys	8.48	2.92	-0.37	1.65×10^{2}	9.10×10^{-5}
		AT-GC	3.78	2.36	-0.13	3.82×10^{4}	2.42×10^{2}
		GC-CG	7.41	3.46	0.00	1.86×10^{-4}	1.86×10^{-4}
	Bottom	AT-Cys	7.36	2.49	-0.50	1.08×10^{5}	3.76×10^{-4}
		GC-Cys	7.87	2.86	-0.37	5.04×10^{4}	2.79×10^{-2}
		CG-Cys	7.96	2.85	-0.37	1.89×10^{3}	1.04×10^{-3}
		AT-GC	3.68	2.32	-0.13	1.29×10^{5}	8.17×10^{2}
		GC-CG	6.75	3.38	0.00	7.66×10^{-4}	7.66×10^{-4}
p21 gene model	Top	AT_1-Cys	8.29	2.54	-0.50	1.36×10^{3}	4.77×10^{-6}
		AT_2-Cys	10.06	2.60	-0.50	4.25	1.49×10^{-8}
		CG-Cys	9.21	2.99	-0.37	1.24	6.83×10^{-7}
		AT_1-AT_2	3.80	2.09	0.00	3.23×10^{4}	3.23×10^{4}
		AT_2-CG	6.55	3.07	-0.13	2.39×10^{1}	1.51×10^{-1}
	Bottom	AT_1-Cys	7.48	2.49	-0.50	8.46×10^{4}	2.96×10^{-4}
		AT_2-Cys	8.66	2.55	-0.50	1.67×10^{4}	5.85×10^{-5}
		CG-Cys	7.72	2.84	-0.37	1.15×10^{3}	6.37×10^{-4}
		AT_1-AT_2	3.68	2.03	0.00	8.20×10^{4}	8.20×10^{4}
		AT_2-CG	6.67	3.09	-0.13	2.36	1.49×10^{-2}

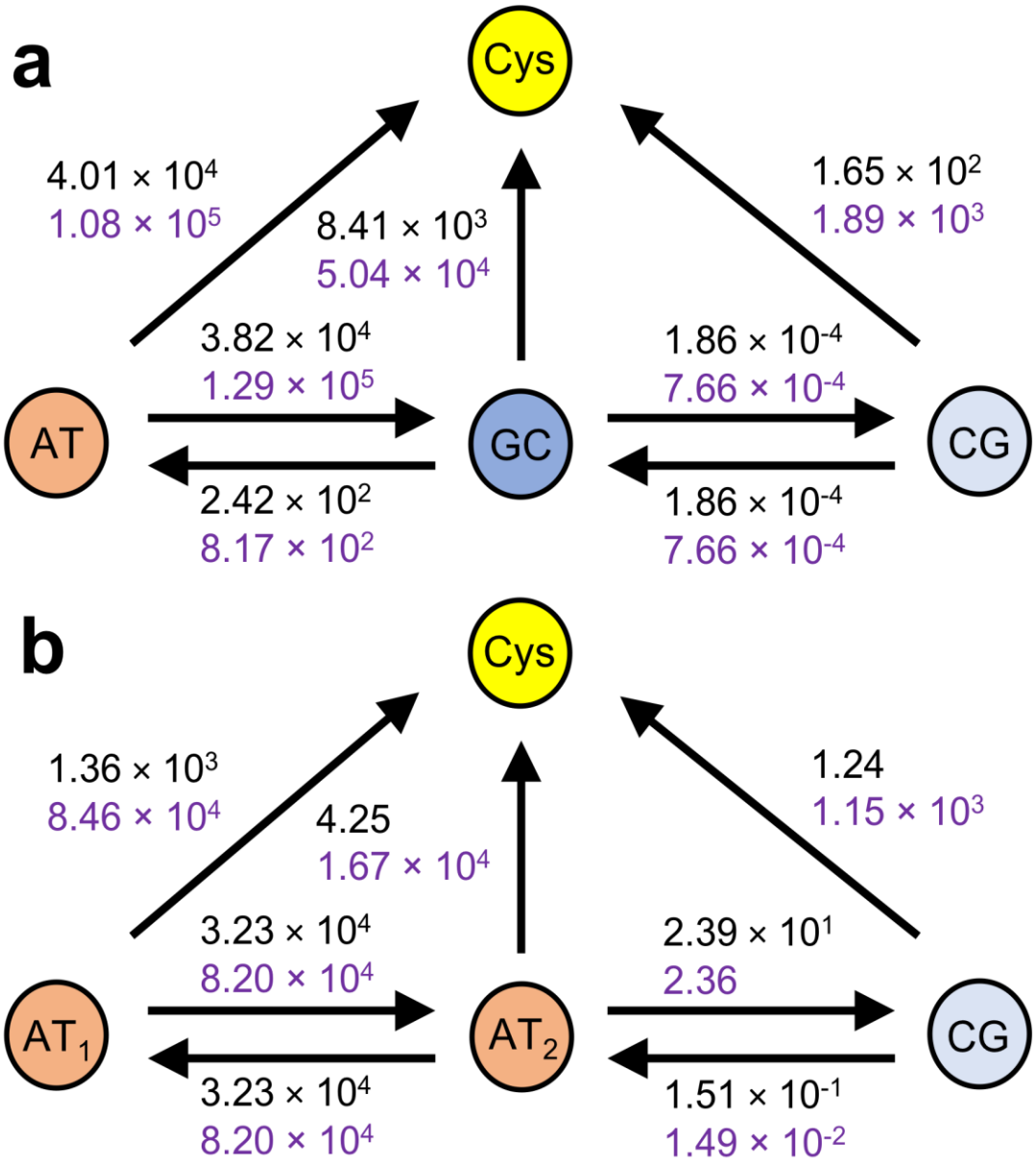

Fig. S8 The CT model systems for the p53-DNA contact region are represented as in Fig. 2 of the article. The value of the hole-transfer rate constants (in s^{-1}) are reported from Table S22.

Table S23 Same properties as in Table 20. $\mathcal{S}_6 = \{\varepsilon_o = 2, \varepsilon_s = 8, R_{\text{bp-bp}} = 3.73\,\text{Å}\}$ was used to obtain the purine effective radii; the dielectric constants $\varepsilon_o = 2.1$ and $\varepsilon_s = 25$ described the p53-DNA interface.

DNA	protein	D-A pair	$\langle R_{DA} \rangle$ (Å)	λ (eV)	$\Delta G°$ (eV)	k_f (s^{-1})	k_b (s^{-1})
Gadd45 gene model	Top	AT-Cys	7.68	2.45	-0.50	6.59×10^{4}	2.31×10^{-4}
		GC-Cys	8.48	2.80	-0.37	2.78×10^{4}	1.54×10^{-2}
		CG-Cys	8.48	2.80	-0.37	5.44×10^{2}	3.01×10^{-4}
		AT-GC	3.78	2.13	-0.13	4.03×10^{5}	2.55×10^{3}
		GC-CG	7.41	3.22	0.00	2.10×10^{-3}	2.10×10^{-3}
	Bottom	AT-Cys	7.36	2.41	-0.50	2.20×10^{5}	7.68×10^{-4}
		GC-Cys	7.87	2.74	-0.37	1.67×10^{5}	9.22×10^{-2}
		CG-Cys	7.96	2.73	-0.37	6.24×10^{3}	3.45×10^{-3}
		AT-GC	3.68	2.08	-0.13	1.36×10^{6}	8.62×10^{3}
		GC-CG	6.75	3.13	0.00	8.68×10^{-3}	8.68×10^{-3}
p21 gene model	Top	AT_1-Cys	8.29	2.51	-0.50	1.75×10^{3}	6.13×10^{-6}
		AT_2-Cys	10.06	2.65	-0.50	2.85	9.96×10^{-9}
		CG-Cys	9.21	2.87	-0.37	4.09	2.26×10^{-6}
		AT_1-AT_2	3.80	1.86	0.00	3.19×10^{5}	3.19×10^{5}
		AT_2-CG	6.55	2.83	-0.13	2.49×10^{2}	1.58
	Bottom	AT_1-Cys	7.48	2.42	-0.50	1.61×10^{5}	5.64×10^{-4}
		AT_2-Cys	8.66	2.54	-0.50	1.82×10^{4}	6.37×10^{-5}
		CG-Cys	7.72	2.72	-0.37	3.81×10^{3}	2.11×10^{-3}
		AT_1-AT_2	3.68	1.80	0.00	8.11×10^{5}	8.11×10^{5}
		AT_2-CG	6.67	2.85	-0.13	2.47×10^{1}	1.56×10^{-1}

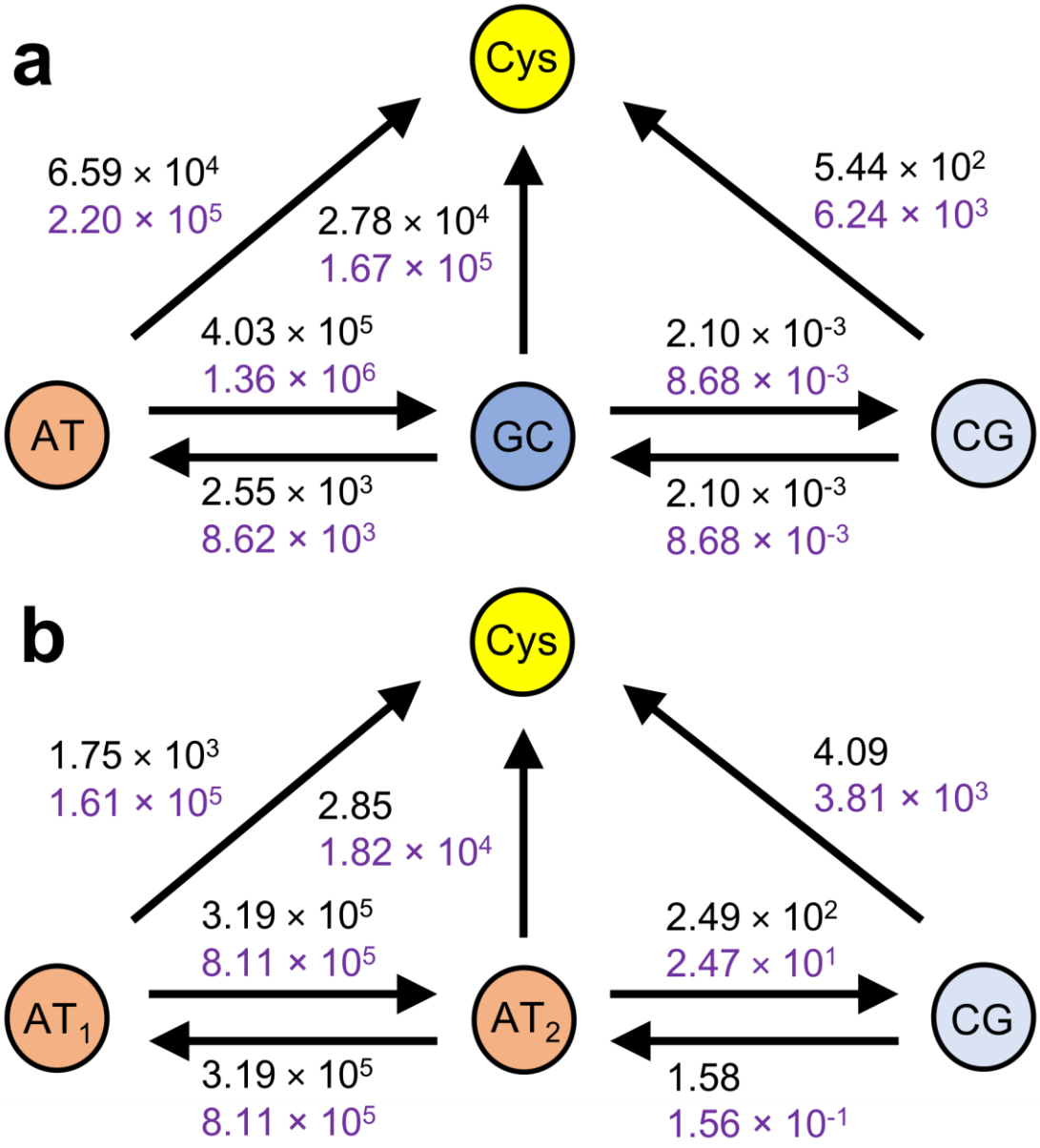

Fig. S9 The CT model systems for the p53-DNA contact region are represented as in Fig. 2 of the article. The value of the hole-transfer rate constants (in s^{-1}) are reported from Table S23.

S5. References

1. J. C. Phillips, R. Braun, W. Wang, J. Gumbart, E. Tajkhorshid, E. Villa, C. Chipot, R. D. Skeel, L. Kalé and K. Schulten, *J. Comput. Chem.*, 2005, **26**, 1781-1802.
2. M. B. Peters, Y. Yang, B. Wang, L. Füsti-Molnár, M. N. Weaver and K. M. Merz, *J. Chem. Theory Comput.*, 2010, **6**, 2935-2947.
3. J. A. Maier, C. Martinez, K. Kasavajhala, L. Wickstrom, K. E. Hauser and C. Simmerling, *J. Chem. Theory Comput.*, 2015, **11**, 3696-3713.
4. A. Pérez, I. Marchán, D. Svozil, J. Sponer, T. E. Cheatham, III, C. A. Laughton and M. Orozco, *Biophys. J.*, 2007, **92**, 3817-3829.
5. J. Wang, P. Cieplak and P. A. Kollman, *J. Comput. Chem.*, 2000, **21**, 1049-1074.
6. W. Jorgensen, J. Chandrasekhar, J. D. Madura, R. W. Impey and M. L. Klein, *J. Chem. Phys.*, 1983, **79**, 926-935.
7. J.-P. Ryckaert, G. Ciccotti and H. J. C. Berendsen, *J. Comput. Phys.*, 1977, **23**, 327-341.
8. T. Darden, D. York and L. Pedersen, *J. Chem. Phys.*, 1993, **98**, 10089-10092.
9. M. Kitayner, H. Rozenberg, N. Kessler, D. Rabinovich, L. Shaulov, T. E. Haran and Z. Shakked, *Mol. Cell*, 2006, **22**, 741-753.
10. A. D. Becke, *J. Chem. Phys.*, 1993, **98**, 5648-5652.
11. A. Migliore, *J. Chem. Phys.*, 2009, **131**, 114113.
12. A. Migliore, *J. Chem. Theory Comput.*, 2011, **7**, 1712-1725.
13. P. H. Dederichs, S. Blügel, R. Zeller and H. Akai, *Phys. Rev. Lett.*, 1984, **53**, 2512-2515.
14. T. A. Wesolowski and A. Warshel, *J. Phys. Chem.*, 1993, **97**, 8050-8053.
15. Q. Wu and T. Van Voorhis, *Phys. Rev. A*, 2005, **72**, 024502.
16. Q. Wu and T. Van Voorhis, *J. Chem. Phys.*, 2006, **125**, 164105.
17. M. Valiev, E. J. Bylaska, N. Govind, K. Kowalski, T. P. Straatsma, H. J. J. Van Dam, D. Wang, J. Nieplocha, E. Apra, T. L. Windus and W. A. de Jong, *Comput. Phys. Commun.*, 2010, **181**, 1477-1489.
18. Y. Mao, Q. Ge, P. R. Horn and M. Head-Gordon, *J. Chem. Theory Comput.*, 2018, **14**, 2401−2417.
19. A. Migliore, S. Corni, D. Varsano, M. L. Klein and R. Di Felice, *J. Phys. Chem. B*, 2009, **113**, 9402-9415.
20. R. Peverati and D. G. Truhlar, *J. Phys. Chem. Lett.*, 2011, **2**, 2810-2817.
21. W. Koch and M. C. Holthausen, *A Chemist's Guide to Density Functional Theory*, Wiley, New York, 2000.
22. A. Migliore, P. H. L. Sit and M. L. Klein, *J. Chem. Theory Comput.*, 2009, **5**, 307-323.
23. R. D. Teo, K. Terai, A. Migliore and D. N. Beratan, *Phys. Chem. Chem. Phys.*, 2018, **20**, 26063-26067.
24. R. A. Marcus and N. Sutin, *Biochim. Biophys. Acta-Rev. Bioenerg.*, 1985, **811**, 265-322.
25. A. M. Kuznetsov and J. Ulstrup, *Electron Transfer in Chemistry and Biology*, John Wiley & Sons, New York, 1999.
26. A. Nitzan, *Chemical Dynamics in Condensed Phases*, Oxford University Press, 2006.
27. K. Siriwong, A. A. Voityuk, M. D. Newton and N. Rosch, *J. Phys. Chem. B*, 2003, **107**, 2595-2601.
28. T. Kubař and M. Elstner, *J. Phys. Chem. B*, 2009, **113**, 5653-5656.
29. H. L. Tavernier and M. D. Fayer, *J. Phys. Chem. B*, 2000, **104**, 11541-11550.
30. G. S. M. Tong, I. V. Kurnikov and D. N. Beratan, *J. Phys. Chem. B*, 2002, **106**, 2381-2392.
31. A. Cuervo, P. D. Dans, J. L. Carrascosa, M. Orozco, G. Gomila and L. Fumagalli, *Proc. Natl. Acad. Sci. U. S. A.*, 2014, **111**, E3624-E3630.
32. G. B. Schuster, *Long-Range Charge Transfer in DNA I*, Springer Science & Business Media, 2004.

33. C. Butchosa, S. Simon and A. A. Voityuk, *Org. Biomol. Chem.*, 2010, **8**, 1870-1875.
34. S. Grimme, J. Antony, S. Ehrlich and H. Krieg, *J. Chem. Phys.*, 2010, **132**, 154104.
35. R. A. Marcus, *J. Phys. Chem.*, 1963, **67**, 853-857.
36. R. A. Marcus, *J. Phys. Chem.*, 1968, **72**, 891-899.
37. A. Migliore, N. F. Polizzi, M. J. Therien and D. N. Beratan, *Chem. Rev.*, 2014, **114**, 3381-3465.
38. A. Khan, *Comput. Theor. Chem.*, 2013, **1013**, 136-139.
39. *Oxygenic Photosynthesis: The Light Reactions*, Springer Netherlands, Dordrecht, The Netherlands, 1996.
40. M. K. Gilson and B. Honig, *Proteins*, 1988, **4**, 7-18.
41. L. Li, C. Li, Z. Zhang and E. Alexov, *J. Chem. Theory Comput.*, 2013, **9**, 2126-2136.
42. A. Heck, P. B. Woiczikowski, T. Kubař, B. Giese, M. Elstner and T. B. Steinbrecher, *J. Phys. Chem. B*, 2012, **116**, 2284-2293.
43. Y. P. Liu and M. D. Newton, *J. Phys. Chem.*, 1995, **99**, 12382-12386.
44. P. Surdhar and D. A. Armstrong, *J. Phys. Chem.*, 1986, **90**, 5915-5917.
45. S. Steenken and S. V. Jovanovic, *J. Am. Chem. Soc.*, 1997, **119**, 617-618.
46. S. Steenken, S. V. Jovanovic, M. Bietti and K. Bernhard, *J. Am. Chem. Soc.*, 2000, **122**, 2373-2374.